Disentangling the Role of the SnO Layer on the Pyro-Phototronic Effect in ZnO-Based Self-Powered Photodetectors

Eliana M. F. Vieira,* José P. B. Silva,* Katarzyna Gwozdz, Adrian Kaim, Nuno M. Gomes, Adil Chahboun, Maria J. M. Gomes, and José H. Correia

Self-powered photodetectors (PDs) have been recognized as one of the developing trends of next-generation optoelectronic devices. Herein, it is shown that by introducing a thin layer of SnO film between the Si substrate and the ZnO film, the self-powered photodetector Al/Si/SnO/ZnO/ITO exhibits a stable and uniform violet sensing ability with high photoresponsivity and fast response. The SnO layer introduces a built-in electrostatic field to highly enhance the photocurrent by over 1000%. By analyzing energy diagrams of the p-n junction, the underlying physical mechanism of the self-powered violet PDs is carefully illustrated. A high photo-responsivity (R) of 93 mA W^{-1} accompanied by a detectivity (D^*) of 3.1×10^{10} Jones are observed under self-driven conditions, when the device is exposed to 405 nm excitation laser wavelength, with a laser power density of 36 mW cm^{-2} and at a chopper frequency of 400 Hz. The Si/SnO/ZnO/ITO device shows an enhancement of 3067% in responsivity when compared to the Al/Si/ZnO/ITO. The photodetector holds an ultra-fast response of ≈ 2 µs, which is among the best self-powered photodetectors reported in the literature based on ZnO.

1. Introduction

Among the various energy detection systems, presently, ultraviolet-visible (UV-Vis) self-powered photodetectors (PDs) have found widespread application in wireless control systems/communication,[1,2] biological/chemical analysis[3,4] visual-image recognition and imaging arrays[5,6] and health in which the UV radiation is responsible for different types of diseases including cataracts and skin cancer.[7,8] In this context, the fabrication of efficient UV-Vis self-powered PDs is necessary.[9]

Recently, the pyro-phototronic effect, has attracted much attention as a promising route/pathway for increasing the PD parameters such as responsivity and detectivity. In this context, self-powered PDs based on ZnO material are attracting tremendous attention.[10,11] In addition to pyroelectric characteristic of the wurtzite ZnO, this material shows multiple properties which make it the excellent candidate for the UV-Vis detection. For instance, ZnO is a cost-effective semiconductor, has direct band-gap ($Eg = 3.37$ eV), strong radiation hardness, high chemical stability, and high room-temperature exciton binding energy (≈ 60 meV).[10]

However, self-powered ZnO-based PDs still suffer from low responsivity and sensitivity. Different approaches, such as nanowires fabrication, doping, and construction of heterojunctions are being employed to improve the self-powered PD characteristics.[11,12] For instance, Wang et al. reported the design and fabrication of a self-powered UV PD based on p-Si/ZnO

E. M. F. Vieira, N. M. Gomes, J.H. Correia
CMEMS – UMinho
University of Minho
Campus de Azurem
Guimarães 4804-533, Portugal
E-mail: evieira@dei.uminho.pt
E. M. F. Vieira, N. M. Gomes, J.H. Correia
LABBELS –Associate Laboratory
Braga, Guimarães, Portugal

The ORCID identification number(s) for the author(s) of this article can be found under https://doi.org/10.1002/smll.202300607.

J. P. B. Silva, M.J.M. Gomes
Physics Center of Minho and Porto Universities (CF-UM-UP)
University of Minho
Campus de Gualtar
Braga 4710-057, Portugal
E-mail: josesilva@fisica.uminho.pt
J. P. B. Silva, M.J.M. Gomes
Laboratory of Physics for Materials and Emergent Technologies
LapMET
University of Minho
Braga 4710-057, Portugal
K. Gwozdz, A. Kaim
Department of Quantum Technologies
Wroclaw University of Science and Technology
Wroclaw 50–370, Poland
A. Chahboun
Université Abdelmalek Essaadi
FST Tanger
Laboratoire Couches Minces et Nanomatériaux (CMN)
Tanger 90000, Morocco

**ADVANCED
SCIENCE NEWS**

www.advancedsciencenews.com

**NANO · MICRO
small**

www.small-journal.com

nanowires (NWs) heterojunction (for 365 nm laser illumination), in which high-performance photodetection has been achieved via induction of the pyroelectric effect on ZnO NWs where the responsivity is enhanced by up to 599% and reaches to 13 mA W^{-1}.[13] Moreover, the response time was improved from 59 µs to 19 µs at the rising edge and from 40 µs to 22 µs at the falling edge. Later, Zhang et al. showed enhanced photodetection of p-Si/n-ZnO NWs (more than 5900%) for a wider spectral range (325 to 785 nm of wavelength) with a maximum responsivity of 79.9 mA W^{-1} for the blue illumination of 442 nm.[13] The response speed of the self-powered PD is shortened from 22.8 to 0.5 ms (rise time) and 7.5 ms to 0.6 ms (fall time). Qiao et al.[14] reported an increment of the photoresponse up to 1580% by the pyro-phototronic effect in the Si/ZnO NWs (400 nm length) and PEDOT:PSS/ZnO NWs (200 nm length) devices with responsivities of 0.565 mA W^{-1} and 0.199 mA W^{-1}, respectively, under zero bias voltage.

Boruah et al.[15] showed an enhancement of 405% in pyrocurrent of halogen-doped ZnO nanorods (NRs) when compared to pristine ZnO NRs, in the absence of external bias voltage. This enhancement is attributed to the tunning of the free charge density of ZnO NRs through the doping of halogen elements. A responsivity of 2.33 mA W^{-1} was reported for the Cl:ZnO NRs photodetector. The nanostructuring of ZnO promote the enlargement of surface-to-volume ratio, which increases the interactive area between light and ZnO and therefore, increases the light absorption which is beneficial to inspire the pyroelectric effect. However, these devices suffer from a weak intrinsic internal electric field at the junction, which results in a lower photoresponsivity.

Tri-layered heterojunctions-based PDs (including Schottky junction, PN junction) attract tremendous attention because the built-in potential in heterostructure can separate the photo-generated electron-hole pairs to achieve self-powered detection without consuming extra power. Recently, Cao et al.[16] demonstrated a ZnO/CuI/Au heterojunction with increased UV detection for self-powering response at 395 nm of laser illumination. The self-powered responsivity of the PD was 61.5 mA W^{-1} and a detectivity of 1.7×10^{10} Jones was achieved. From the response, a rise/fall time of 0.08 s/0.41 s, respectively, was observed. Moreover, the influence of thermal treatment on ZnO films in p-NiO/n-ZnO PDs was proposed and the photoresponse to a 365 nm laser illumination was systematically investigated.[17] The pyrocurrent magnitude is enhanced by 1264.41% for the thermally treated device. The thermally treated device exhibits high responsivity and detectivity of 0.29 A W^{-1} and 2.75×10^{11} Jones, respectively. An ultrafast response speed with rise time of 3.92 µs and a fall time of 8.90 µs is achieved. Another tri-layered device with Si/Ag/ZnO can also make use of the pyro-phototronic effect to boost photoresponse of the device. When illuminated under a 405 nm laser (5 mW cm^{-2}) and at a chopper frequency of 825 Hz, ultra-fast rise time of 20 µs was obtained, which is 6 times higher than that of the Si/ZnO PD.[18] Recently, we demonstrated that a n-p-n heterojunction is a promising solution for self-powered PDs.[20] A tri-layered heterojunction of n-Si/p-SnO$_x$/n-ZnO shows a responsivity of 36.7 mA W^{-1} with a detectivity of 1.5×10^{11} Jones. Ultra-fast rise and fall times of 3 and 2 µs were also achieved, respectively. However, the responsivity of the PD is limited by the formation

of a SnO$_x$ layer which consists of a mixture of phases (p-type SnO, n-type SnO_2, and Sn) This degrades the p-n junction between the SnO$_x$ and the ZnO layers as well as SnO$_x$ and Si, which makes the electron-hole recombination more likely and the separation of the carriers less efficient.

Therefore, in this work, we demonstrate the PD performance improvement in the Si/ZnO heterojunction through the insertion of a p-type pure SnO layer between Si and ZnO thin film. P-type pure of SnO layer can be optimized by its own thickness.[19] Therefore, in this work, a 25 nm thick SnO layer was used to fabricate the n-p-n heterojunction. We systematically investigated the photoresponse of the developed PD under different chopping frequencies and different power densities with a 405 nm laser illumination. Moreover, the PD performance is compared with the one obtained for a p-Si/n-ZnO PD in order to unravel the role of the SnO layer on the PD behavior.

2. Experimental Section

The growth conditions for the Al/Si/SnO/ZnO/ITO device was previously reported.[20] However, the Sn deposition time was further optimized to achieve a 25-nm thick film.

The crystal structures of the Si/SnO/ZnO and Si/ZnO films were characterized using X-ray diffraction (XRD). A Bruker D8 Advance DaVinci (Germany) diffractometer at room-temperature over the 2θ range = 15–65°; step size: 0.04°/1 s, in a Bragg-Brentano configuration using CuKα radiation (λ = 1.5406 Å) was used. The Si/SnO/ZnO heterostructure and surface morphology were evaluated by using a field-emission scanning electron microscope (FE-SEM: Auriga Compact-Zeiss). The PVE300 photovoltaic QE system from Bentham was used for the external quantum efficiency (EQE) determination. $I(t)$ characteristic curves were measured by a self-made setup consisting of National Instruments acquisition card 6251 (pulse generation and data acquisition) and Keithley 428 Current Amplifier. The violet light source was provided by a semiconductor laser with a wavelength of 405 nm and power in the range of 7.1 up to 43.3 mW, controlled with a TTL signal. The effect of the chopper frequency was investigated by using a pulsed repetition rate of 10 Hz, 100 Hz, 200 Hz, 300 Hz, and 400 Hz, respectively. Moreover, the photodetectors were illuminated under different power densities of laser of 405 nm, namely 36 mW cm^{-2}, 87 mW cm^{-2}, 133 mW cm^{-2}, 178 mW cm^{-2}, and 221 mW cm^{-2}.

3. Results and Discussion

The XRD spectra of the Si/ZnO and Si/SnO/ZnO heterostructures with a 2θ scanning angle ranging from 15° to 65° are given in **Figure 1**a. The wurtzite phase of ZnO is present in the Si/ZnO heterostructure, while the tetragonal SnO and wurtzite ZnO phases are found to be present in the Si/SnO/ZnO heterostructure. The top-view and side-view high-resolution scanning electron microscopy (HRSEM) images of the Si/SnO/ZnO heterojunction are shown in Figure 1b. From the cross-sectional image, the thickness of SnO and ZnO films is ≈25 ± 5 nm and 45 ± 5 nm, respectively. ZnO film forms a compact structure, while a granular layer is observed for the SnO film. Moreover,
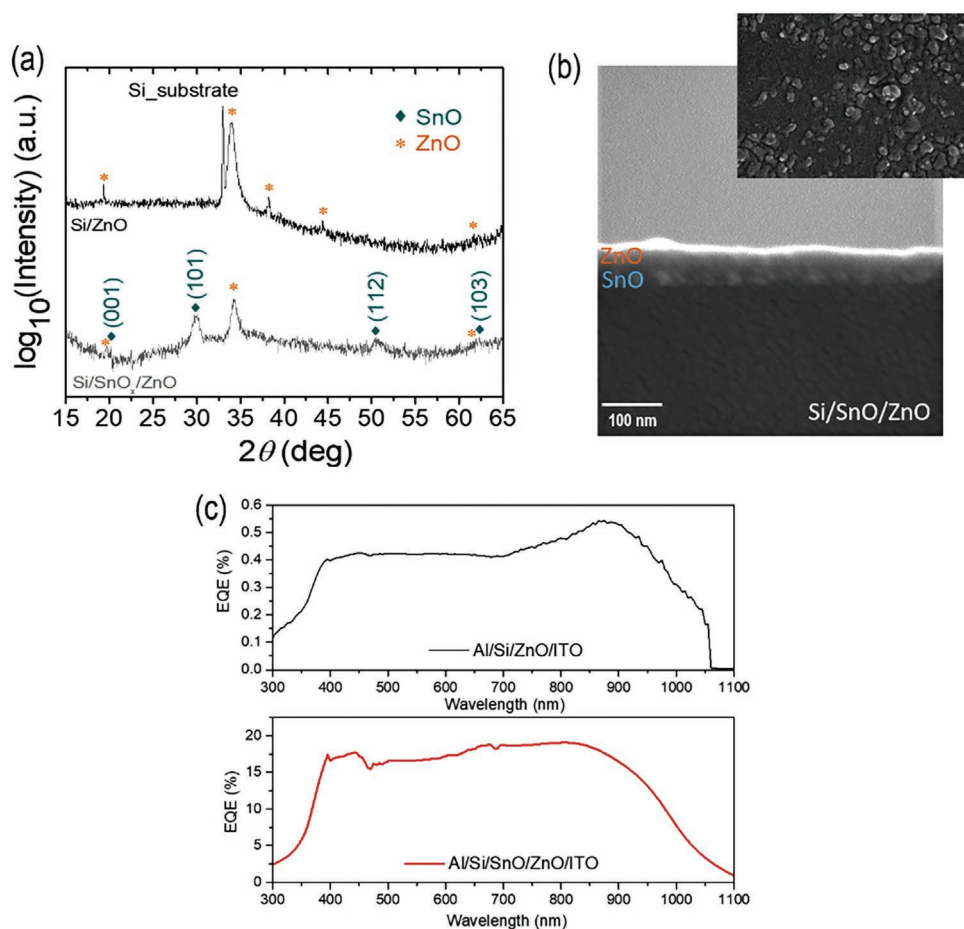
Figure 1. a) XRD spectra of the Si/ZnO and Si/SnO/ZnO heterojunctions; b) cross-sectional and top-view (in the inset) scanning electron micrograph images of the Si/SnO/ZnO heterojunction and c) external quantum efficiency (EQE) as a function of the wavelength for the Al/Si/SnO/ZnO/ITO device compared to the Al/Si/ZnO/ITO device.

as it can be seen in the inset of Figure 1b, some aggregations of large particles with clear edges were observed in the surface morphology of the ZnO layer, but without any visible cracks. The external quantum efficiency (EQE) as a function of light wavelength is shown in Figure 1c. Maximum EQE values of 19% and 0.5% for Al/Si/SnO/ZnO/ITO and Al/Si/ZnO/ITO photodetectors are observed, respectively. Both structures exhibit the rectangular shape of the EQE curve, so they are sensitive to a wide range of visible wavelengths. The EQE response for wavelengths 300–350 nm is reduced due to the high surface recombination. The increase of the EQE values for all the wavelengths is due to better carrier separation at the SnO/Si junction.

In order to unravel the role of the introduction of the SnO layer in the heterojunction, **Figure 2** shows the band diagrams for both structures. In Figure 2a the junction between p-Si and n-ZnO is presented. The values for Si are calculated from parameters given by the producer.[20] The band gap for ZnO was determined experimentally.[21] Comparing with the junction between n-Si and p-SnO (Figure 2b), it is clear that the band offset is really low in this case. The parameters are calculated the same way as in Figure 2a. The built-in potential is calculated from current-voltage characteristics. In Figure 2c the photocarriers generation at the n-ZnO/p-Si junction is presented.

405 nm wavelength is absorbed in the Si substrate. The electrons are excited into the conduction band and the hole appears in the valance band. The built-in electric field at the junction is separating the carriers. However, the valance band offset between ZnO and Si is ≈2.5 eV. It can increase the recombination, lower the carriers separation and decrease the efficiency and the EQE of the junction.[22] In Figure 1d the n-ZnO/p-SnO/n-Si junction is shown. Two p-n junctions must be considered. Photogeneration occurs in SnO layer as the energy gap allows it to absorb the 405 nm wavelengths. The generated carriers are separated by the built-in electric field (E_{bi2}). Electrons flow freely into the electrode; however, the holes are accumulating at the ZnO/SnO junction, because of the presence of the E_{bi1}. The increase of the EQE in structure Al/Si/SnO/ZnO/ITO compared to Al/Si/ZnO/ITO (Figure 1c) proves that the E_{bi1} is smaller than E_{bi2}. Otherwise, the carrier separation would not be efficient.

The $I(t)$ response for different chopper frequencies (from 10 up to 400 Hz), at zero bias for a fixed power density of 221 Mw cm^{-2} and by using a 405 nm light illumination, of the Al/Si/ZnO/ITO and Al/Si/SnO/ZnO/ITO PDs is illustrated in **Figure 3**a,b. The layout of the fabricated devices, which have a sandwich structure configuration, are also shown above each
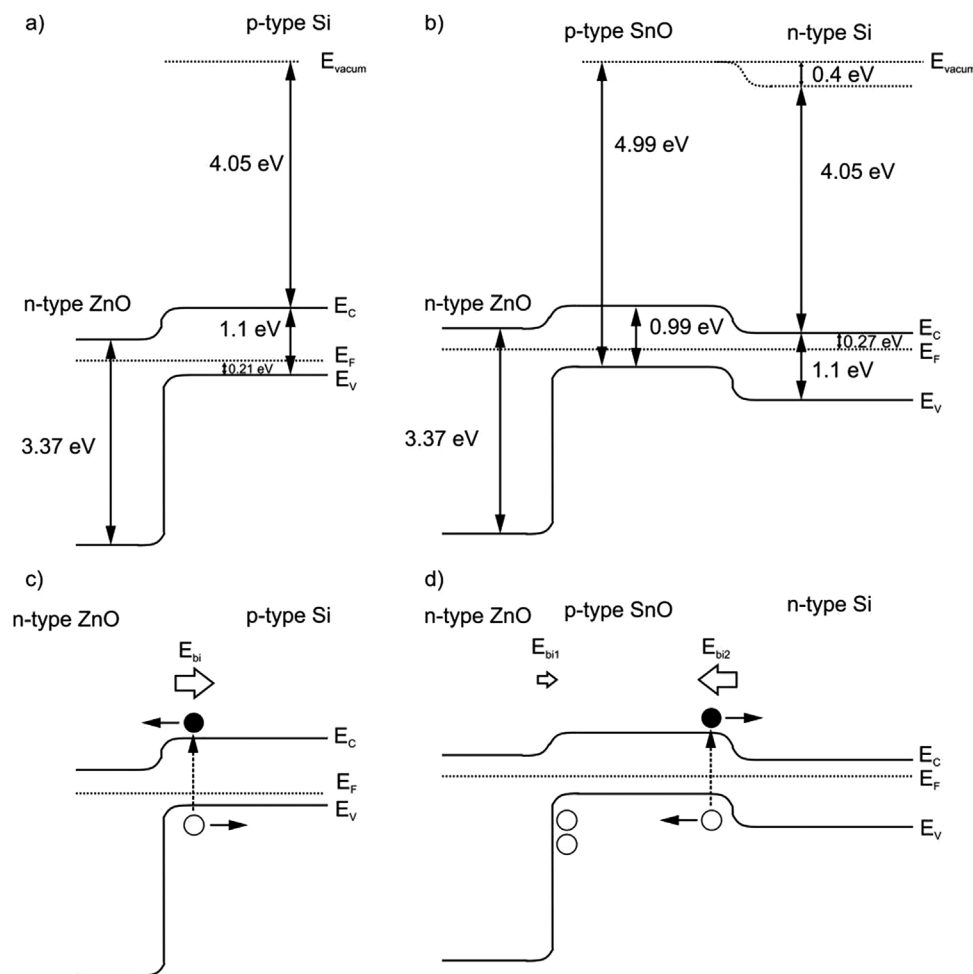
Figure 2. Band diagrams for a) p-Si/ZnO and b) n-Si/SnO/ZnO heterojunctions, photocarriers generation, the electric fields and accumulation of holes for c) p-Si/ZnO and d) n-Si/SnO/ZnO heterojunctions.

$I(t)$ graph. The $I(t)$ curves show a typical sharp increase in the current when the light is turned on due to the pyro-phototronic effect, which is observed for all fixed frequencies and for the two devices. As illustrated in the Figure 3b, the current in the Al/Si/SnO/ZnO/ITO photodetector rapidly increases and reaches a maximum value of 0.7 mA for 400 Hz of chopper frequency, being ≈10 times more than the maximum current value shown by the Al/Si/ZnO/ITO device (see Figure 3a). This is a consequence of using a pure p-type SnO layer in the Al/Si/SnO/ZnO/ITO device, as corroborated by the XRD analysis. Compared to the previous work,[20] the *p-n* quality of the junction is improved, and then, the built-in electric field is higher at the interface and the separation of the carriers is more efficient, which leads to a higher photocurrent. In addition, and similarly to what was observed in the ZnO/NiO/Si heterojunction,[23] the SnO barrier layer plays a crucial role in modulating carrier transport and improving the pyro-phototronic effect for the performance enhancement of the PDs by effectively reducing the electron current, as shown in Figure S1, Supporting information. Figure 3c shows the expanded dynamic behavior of the four-stage photoresponse behavior, with a single-cycle transient response and the contribution of both the photovoltaic

and pyroelectric output current signals. The mechanism of the pyro-phototronic effect is as follows: when the illumination is turned on, there is an increase in the transient temperature of the device ($dT/dt > 0$) producing a pyroelectric polarization potential (V_{Pyro} (E_{pyro})) in the ZnO, which promotes the separation of photogenerated carriers and hence producing a pyroelectric current (I_{pyro}). In this sense, a fast spike in the output current is observed ($I_{pyro+Photo}$). Owing to the gradually decrease of the temperature variation ($dT/dt = 0$), V_{Pyro} disappears progressively, which leads to the decrease of the I_{Pyro}, and then the output current originates only from the photovoltaic effect, I_{Photo}. Upon switching OFF the illumination, a reduction in the transient temperature ($dT/dt < 0$) results in V_{pyro} in opposite direction to the light-induced V_{photo}. Consequently, a strong and negative current is observed, owing to the reversed pyro-charges. Afterward, the temperature of the device tends to stabilize at room temperature ($dT/dt = 0$), and therefore I_{pyro} vanishes and the output current returns to a stable value near zero (dark current, I_{dark}). The corresponding currents $I_{pyro+Photo}$ and I_{Photo} are extracted from the Al/Si/ZnO/ITO and Al/Si/SnO/ZnO/ITO devices are plotted in Figure 3d,e, respectively. While the I_{Photo} (dark squares) is almost chopper frequency

ADVANCED
SCIENCE NEWS
www.advancedsciencenews.com

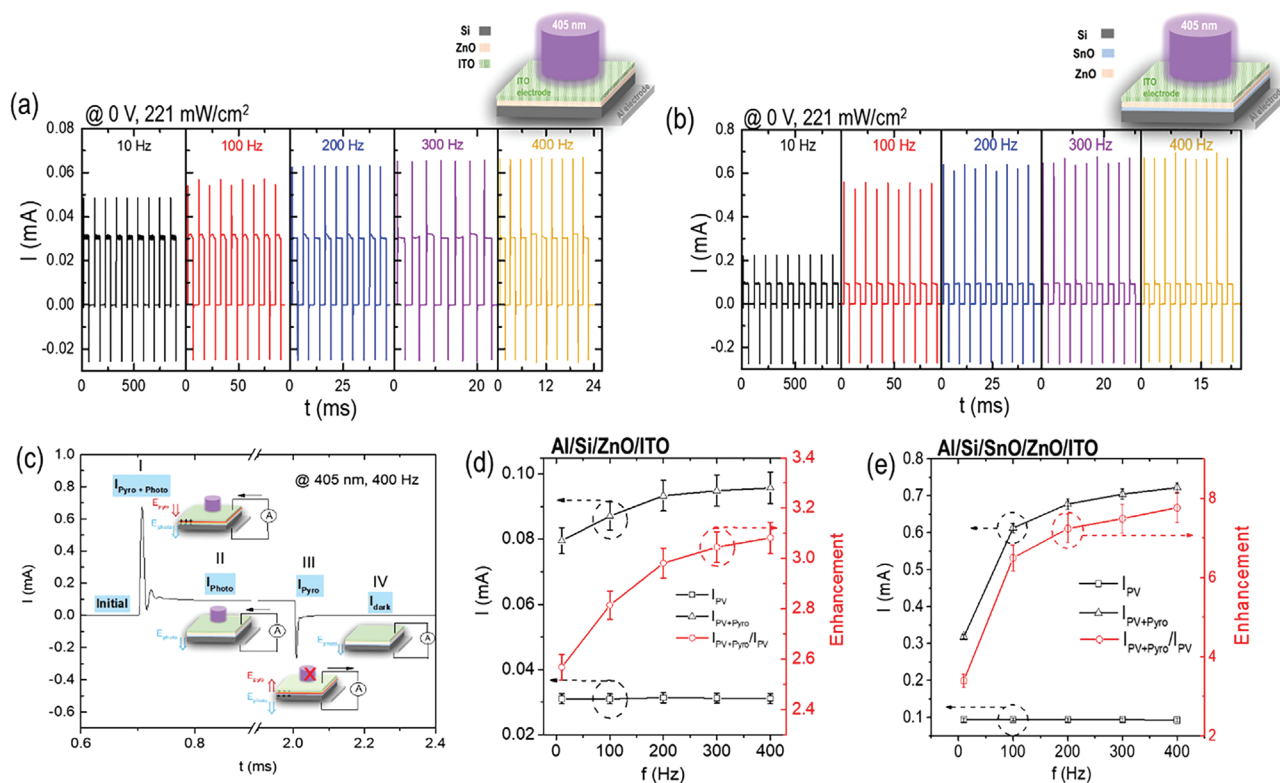NANO · MICRO
small
www.small-journal.com

Figure 3. Systematic detailed transient responses of the UV self-powered a) Al/Si/ZnO/ITO and b) Al/Si/SnO/ZnO/ITO devices at different chopper frequencies and at a fixed power density of 221 mW cm^{-2}. The illustration of each device structure is shown above each graph. c) Typical transient response of the device with 405 nm laser illumination for 400 Hz chopper frequency with a schematic representation of the current generation, as a result of pyroelectric polarization arising by the light-induced transient heating effect. d,e) Output current ($I_{Pyro+Photo}$), photovoltaic current (I_{Photo}), enhancement factor by the pyroelectric effect ($I_{Pyro+Photo}/I_{Photo}$), as a function of chopper frequency (10 to 400 Hz), for the two devices. The error bars represent the standard deviation of the data.

independent for the two devices as expected, the $I_{pyro+Photo}$ (dark triangles) increases with the chopper frequency increment. Considering the high heating rate dT/dt of light, as the chopper frequency increases, E_{pyro} increases, and thus the $I_{pyro+Photo}$ is higher. As a consequence, $I_{pyro+Photo}/I_{Photo}$ (red circles) increases almost 3.1 times for the Al/Si/ZnO/ITO device (Figure 3d) and 7.7 times for the Al/Si/SnO/ZnO/ITO device (Figure 3e), at 400 Hz of chopper frequency.

The $I(t)$ response for different visible laser wavelengths (405, 515, and 650 nm), with a chopper frequency of 400 Hz, at zero bias for a fixed power density of 250 mW cm^{-2}, are now given in Figure S2, Supporting information. From this figure, it is possible to observe that I_{PV} is almost laser wavelength independent, while I_{Pyro} significantly increases with the laser wavelength. With increasing the laser wavelength increases, the temperature gradient between the ZnO surfaces is higher and therefore $I_{Pyro+PV}$ is also higher.[24]

On the other hand, by varying the power densities from 36 to 221 mW cm^{-2}, the transient response characteristics of the fabricated Al/Si/ZnO/ITO and Al/Si/SnO/ZnO/ITO devices were systematically investigated and summarized in **Figure 4**a,b, respectively. As it is possible to observe from the $I(t)$ curves, the pyro-phototronic effect occurs for all the different laser power densities. A significant degradation of the photovoltaic characteristics of the Al/Si/ZnO/ITO is observed with the decrease of

the illumination power (Figure 4a). Interestingly, this behavior is not observed in the Al/Si/SnO/ZnO/ITO device (Figure 4b). This strongly suggests that the detrimental effect can be avoided by controlling the interfacial design, indicating that the Si/SnO interface play crucial role in creating high photocurrent (compare with Figure 1c) through efficient carriers separation. In addition, in AC photovoltaic effect, the magnitude of the current increases with increasing the light power. This reveals that the electrical output is strongly associated with light absorption and the total amount of light-excited charge carriers.[25] In our case, as shown in Figure 4d, the current increases with decreasing the light power. Therefore, the observed current is due to the pyro-phototronic effect.

The $I_{Pyro+Photo}$, I_{Photo}, and the ratio between them ($I_{Pyro+Photo}/I_{Photo}$) as a function of the power density illuminations, for the two devices, are shown in Figure 4c,d. Both $I_{Pyro+Photo}$ (dark triangles) and I_{Photo} (dark squares) increase with the stimulating power density increasing from 36 mW cm^{-2} to 221 mW cm^{-2} for Al/Si/ZnO/ITO device (Figure 4c). However, as can be seen in Figure 4d for the Al/Si/SnO/ZnO/ITO device, $I_{Pyro+Photo}$ (dark triangles) is found to increase with increasing laser power density at low laser powers from 36 mW cm^{-2} to 87 mW cm^{-2}, but it then decreases from 87 mW cm^{-2} to 221 mW cm^{-2}. On the other hand, I_{Photo} (dark squares) increased moderately as laser power density increased. It is
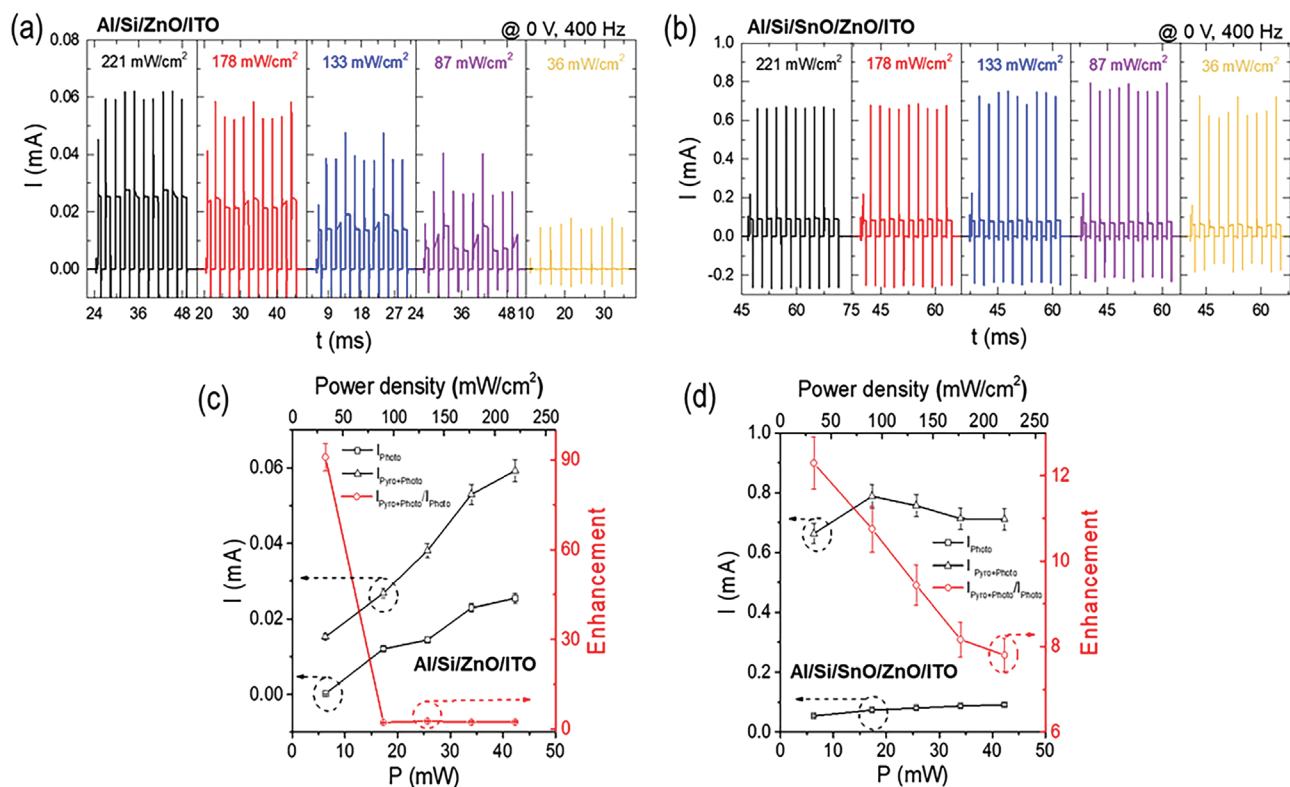
Figure 4. Systematic detailed transient responses of the UV self-powered a) Al/Si/ZnO/ITO and b) Al/Si/SnO/ZnO/ITO devices at different laser power densities, and at a fixed chopper frequency of 400 Hz. Variation of $I_{Pyro+Photo}$, I_{Photo}, and $I_{Pyro+Photo}/I_{Photo}$ for c) Al/Si/ZnO/ITO and d) Al/Si/SnO/ZnO/ITO devices, as a function of laser power density (36 to 221 mW cm^{-2}). The error bars represent the standard deviation of the data.

noteworthy to point out that the $I_{Pyro+Photo}/I_{Photo}$ ratio (red circles) increases linearly after decreasing the laser power density from 221 to 36 mW cm^{-2}, which can be attributed to a decrease in I_{Photo} and not to a decrease in I_{Pyro}.

The photodetectors performance was evaluated by estimating the responsivity (R), detectivity ($D*$), and sensitivity (S) according to Equations (1), (2), and (3):

$$R = \frac{I_{light} - I_{dark}}{P} \tag{1}$$

$$D* = R\left(\frac{A}{2qI_{dark}}\right)^{1/2} \tag{2}$$

$$S = \frac{I_{light} - I_{dark}}{I_{dark}} \tag{3}$$

in which I_{Light} and I_{dark} are the current with and without illumination, respectively. P and A are the effective illumination power and area on the device, respectively, and q represents electronic charge. It is possible to observe that R, $D*$, and S increase with chopper frequency for the two devices (**Figure 5**a,b). For the chopper frequency of 400 Hz, R, $D*$, and S reach, respectively, values of 13.5 mA W2212, 3.0 ×10^{10} Jones and 14 900 for Al/Si/ZnO/ITO device and 103 mA/W, 3.4 ×10^{10} Jones and 2500 for Al/Si/SnO/ZnO/ITO device, respectively. Particularly, at a higher chopper frequency of 400 Hz, a ~763% enhancement in

R is observed when the SnO layer is introduced in the Al/Si/ZnO/ITO photodetector structure (Figure 5b). Moreover, while the R of the device without SnO layer is almost constant with chopper frequency increasing, the results show that the R of Al/Si/SnO/ZnO/ITO device at a high chopper frequency of 400 Hz could be nearly 2 times as large as that at a low chopper frequency of 10 Hz. Furthermore, the R, $D*$, and S parameters were estimated as a function of the laser power density and are shown in Figure 5c,d. No significant variation is observed in the R and $D*$ for Al/Si/ZnO/ITO device. On the other hand, for the Al/Si/SnO/ZnO/ITO device, R and $D*$ parameters increase with a decrease of the laser power density and they reach 93.0 mA W^{-1} and 3.1 × 10^{10} Jones, respectively, with a laser power density of 36 mW cm^{-2}. The device with the SnO layer shows an enhancement of 3067% in responsivity when compared to the Al/Si/ZnO/ITO. Moreover, the S parameter tends to increase with a decrease in the laser power density from 221 up to 87 mW cm^{-2} for Al/Si/ZnO/ITO device, while a slight decrease was observed for 36 mW cm^{-2} due to the decrease in the I_{Pyro} and I_{PV}, as already observed in Figure 4d. Moreover, the photovoltaic degradation observed in Al/Si/ZnO/ITO device with the decreasing of density power leads to a decrease of S. A maximum sensitivity of 2700 was achieved at 87 mW cm^{-2} for the device with the SnO/ZnO heterojunction.

The effect of the chopper frequency and the laser power density on rise time (τ_{rise}) and fall time (τ_{fall}) were investigated for the two photodetectors, with and without the SnO layer, and are shown in **Figure 6**. A clear improvement of the response time
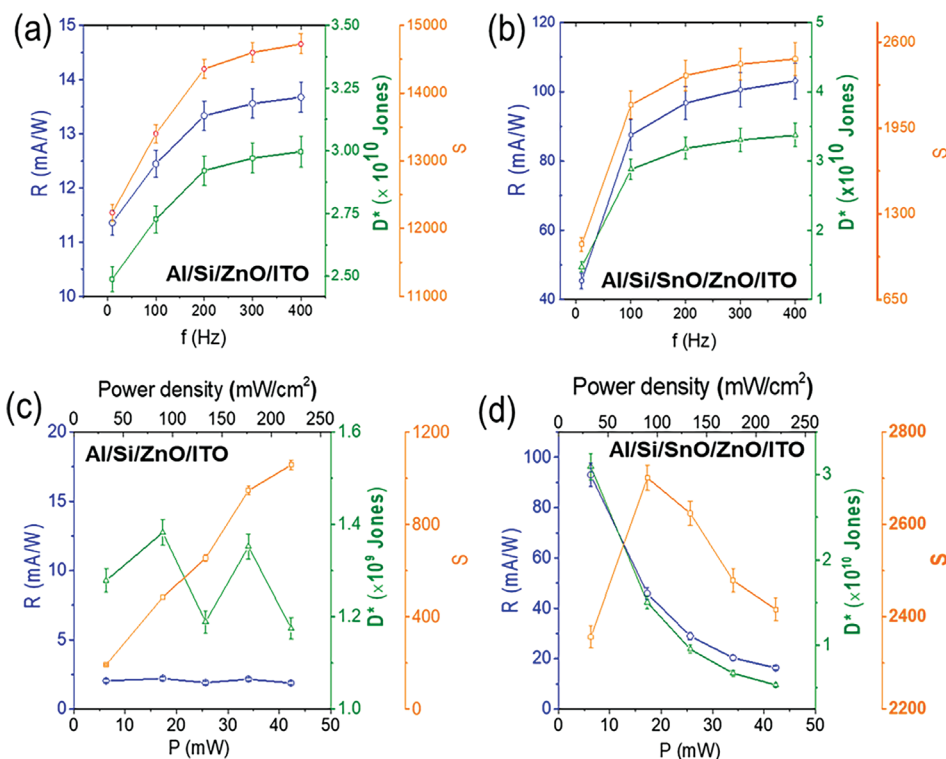
**ADVANCED
SCIENCE NEWS**

www.advancedsciencenews.com

NANO · MICRO

small

www.small-journal.com

Figure 5. Responsivity (*R*), detectivity (*D**), and sensitivity (*S*), as a function of chopper frequency from a,b) 10 to 400 Hz and c,d) power density ,for the Al/Si/ZnO/ITO and Al/Si/SnO/ZnO/ITO devices, respectively. The error bars represent the standard deviation of the data.
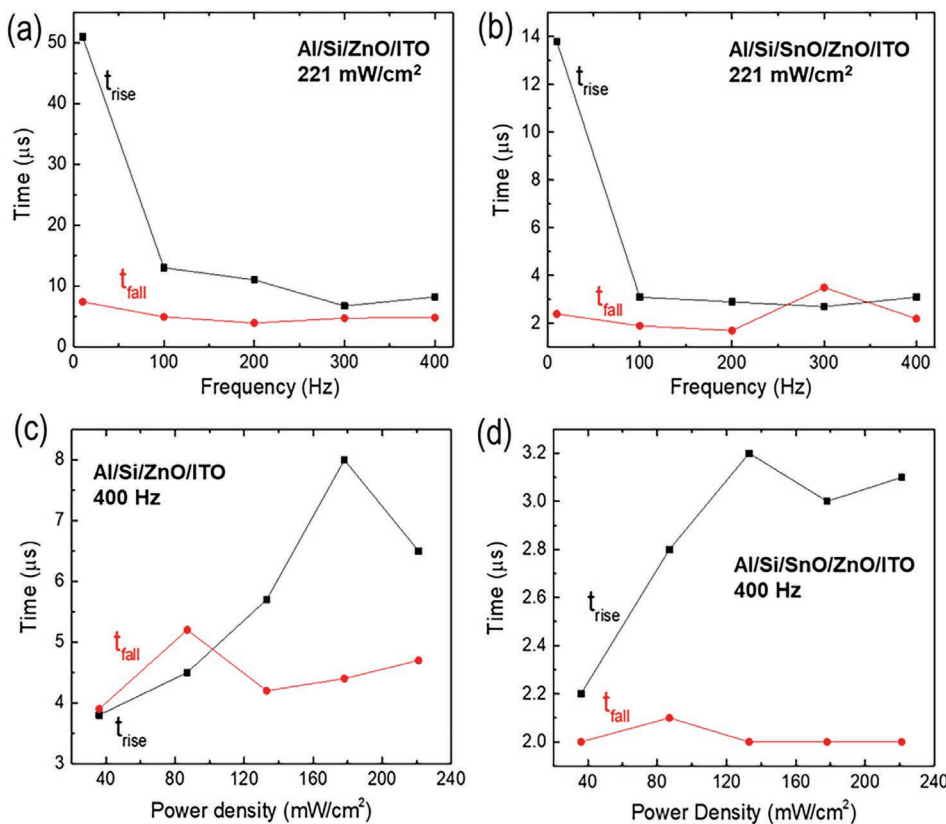

Figure 6. The corresponding rise times (τ_{rise}) and fall times (τ_{fall}) change when the self-powered Al/Si/ZnO/ITO and Al/Si/SnOx/ZnO/ITO devices are irradiated by a,b) different chopper frequencies and c,d) power densities respectively.

ADVANCED
SCIENCE NEWS
www.advancedsciencenews.com

NANO · MICRO
small
www.small-journal.com

was observed with the introduction of the SnO layer in the ZnO photodetector structure. Under zero bias and at a chopper frequency of 400 Hz, the rise time decreased from 8.2 to 3.1 µs and the fall time also decreased from 4.8 to 2.2 µs. Moreover, at the lowest power density (36 mW cm^{-2}) a ultrafast response speed of 2.2 µs/2.0 µs (rise time/fall time) is observed for the Al/Si/SnO/ZnO/ITO device in contrast with the response speed of 3.8 µs/3.9 µs (rise time/fall time) evidenced for the Al/Si/ZnO/ITO device.

The present Al/Si/SnO/ZnO/ITO PD performance exhibits 5-order of magnitude faster rise and fall time with 405 nm laser illumination when compared to the recent work of K. Zhao et al.[26] and 1-order of magnitude higher responsivity and 3-orders of magnitude faster response when compared to plasmon-induced pyro-phototronic effect in ZnO/CuO p-n junctions,[27] suggesting that the n-p-n heterojunction based on n-Si/p-SnO/n-ZnO is a promising solution for photosensing.

4. Conclusions

In summary, we successfully fabricated a self-powered and ultra-fast Al/Si/SnO/ZnO/ITO photodetector which relies on the pyro-phototronic effect. The photoresponse of the device to 405 nm laser illumination, with and without the SnO layer, has been carefully investigated as a function of the chopper frequency and the incident light power density. We showed an order-of-magnitude enhancement in photocurrent generation by the introduction of a 25 nm-thick SnO layer in the Al/Si/ZnO/ITO device. The Al/Si/SnO/ZnO/ITO device exhibits an optimum responsivity and detectivity of 93 mA W^{-1} and 3.1×10^{10} Jones, respectively, with a laser power density of 36 mW cm^{-2} and at a chopper frequency of 400 Hz. Ultrafast rise and fall times of 2.2 and 2.0 µs, respectively, were obtained. The boosted performance could be attributed to the high-quality n-Si/p-SnO/n-ZnO heterojunction that provides a higher separation efficiency of carriers due to built-in electric field at the interface. Thus, excellent photoresponse performance is realized. This work offers a simple and effective method to achieve high-performance and self-powered photodetectors which are highly desirable in the fields of image recognition, optoelectronic systems, and biological chemical sensors.

Supporting Information

Supporting Information is available from the Wiley Online Library or from the author.

Conflict of Interest

The authors declare no conflict of interest.

Author Contributions

E.M.F. V. and J.P.B.S. contributed equally to this work. Eliana M. F. Vieira: Conceptualization, Methodology, Validation, Investigation, Formal Analysis, Writing – original draft. José P. B. Silva: Methodology, Validation, Investigation, Formal analysis, Writing – Review & Editing. Katarzyna Gwozdz: Investigation, Formal analysis. Adrian Kaim: Investigation. Nuno M. Gomes: Methodology. Adil Chahboun: Conceptualization, Writing – Review & Editing. Maria J.M. Gomes: Resources, Supervision. José H. Correia: Resources, Supervision, Writing – Review & Editing.

Data Availability Statement

The data that support the findings of this study are available from the corresponding author upon reasonable request.

[1] H. Guan, D. Lv, T. Zhong, Y. Dai, L. Xing, X. Xue, Y. Zhang, Y. Zhan, *Nano Energy* **2020**, *67*, 104182.

[2] T. Ouyang, X. Zhao, X. Xun, B. Zhao, Z. Zhang, Z. Qin, Z. Kang, Q. Liao, Y. Zhang, *Adv. Funct. Mater.* **2022**, *32*, 2202184.

[3] S. Khan, D. Newport, S. Le Calvé, *Sensors* **2019**, *19*, 5210.

[4] W. Ouyang, F. Teng, X. Fang, *Adv. Funct. Mater.* **2018**, *28*, 1707178.

[5] Y. Dai, Y. Fu, H. Zeng, L. Xing, Y. Zhang, Y. Zhan, X. Xue, *Adv. Funct. Mater.* **2018**, *28*, 1800275.

[6] M. Wang, J. Zhang, Q. Xin, L. Yi, Z. Guo, Y. Wang, A. Song, *Opt. Express* **2022**, *30*, 27453.

[7] Z. Zhang, Y. Geng, S. Cao, Z. Chen, H. Gao, X. Zhu, X. Zhang, Y. Wu, *ACS Appl. Mater. Interfaces* **2022**, *14*, 41257.

[8] F. Zölzer, S. Bauer, *Int. J. Environ. Res. Public Health* **2021**, *18*, 4887.

[9] J. P. B. Silva, K. Gwozdz, L. S. Marques, M. Pereira, M. J. M. Gomes, J. L. MacManus-Driscoll, R. L. Z. Hoye, *Carbon Energy* **2022**, *1*.

[10] Z. Xu, Y. Zhang, Z. Wang, *J. Phys. D: Appl. Phys.* **2019**, *52*, 223001.

[11] W. Ouyang, J. Chen, Z. Shi, X. Fang, *Appl. Phys. Rev.* **2021**, *8*, 031315.

[12] V. Panwar, S. Nandi, M. Majumder, A. Misra, *J. Mater. Chem. C* **2022**, *10*, 12487.

[13] Y. Zhang, M. Hu, Z. Wang, *Nano Energy* **2020**, *71*, 104630.

[14] S. Qiao, H. Sun, J. Liu, G. Fu, S. Wang, *Nano Energy* **2022**, *95*, 107004.

[15] B. Deka Boruah, S. Naidu Majji, S. Nandi, A. Misra, *Nanoscale* **2018**, *10*, 3451.

[16] F. Cao, L. Jin, Y. Wu, X. Ji, *J. Alloys Compd.* **2021**, *859*, 158383.

[17] A. K. Rana, M. Kumar, D. Ban, C. Wong, J. Yi, J. Kim, *Adv. Electron. Mater.* **2019**, *5*, 1900438.

[18] Y. Zhu, B. Wang, C. Deng, Y. Wang, X. Wang, *Nano Energy* **2021**, *83*, 105801.

[19] E. M. F. Vieira, J. P. B. Silva, K. Veltruská, V. Matolín, A. L. Pires, A. M. Pereira, M. J. M. Gomes, L. M. Goncalves, *Nanotechnology* **2019**, *30*, 435502.

[20] J. P. B. Silva, E. M. F. Vieira, J. M. B. Silva, K. Gwozdz, F. G. Figueiras, K. Veltruská, V. Matolín, M. C. Istrate, C. Ghica, K. C. Sekhar, A. L. Kholkin, L. M. Goncalves, A. Chahboun, M. Pereira, *J. Mater. Chem. A* **2020**, *8*, 11314.

[21] E. M. F. Vieira, J. P. B. Silva, K. Veltruská, C. M. Istrate, V. Lenzi, V. Trifiletti, B. Lorenzi, V. Matolín, C. Ghica, L. Marques, O. Fenwick, L. M. Goncalves, *ACS Appl. Mater. Interfaces* **2021**, *13*, 35187.

[22] R. Pietruszka, R. Schifano, T. A. Krajewski, B. S. Witkowski, K. Kopalko, L. Wachnicki, E. Zielony, K. Gwozdz, P. Bieganski, E. Placzek-Popko, M. Godlewski, *Sol. Energy Mater. Sol. Cells* **2016**, *147*, 164.

[23] B. Yin, H. Zhang, Y. Qiu, Y. Luo, Y. Zhao, L. Hu, *Nanoscale* **2017**, *9*, 17199.

[24] J. P. B. Silva, E. M. F. Vieira, K. Gwozdz, A. Kaim, L. M. Goncalves, J. L. MacManus-Driscoll, R. L. Z. Hoye, M. Pereira, *Nano Energy* **2021**, *89*, 106347.

[25] H. Zou, G. Dai, A. C. Wang, X. Li, S. L. Zhang, W. Ding, L. Zhang, Y. Zhang, Z. L. Wang, *Adv. Mater.* **2020**, *32*, 1907249.

[26] K. Zhao, B. Ouyang, C. R. Bowen, Y. Yang, *Nano Energy* **2020**, *77*, 105152.

[27] Q. Li, J. Meng, J. Huang, Z. Li, *Adv. Funct. Mater.* **2022**, *32*, 2108903.